DOI: https://doi.org/10.24425/amm.2025.154460

LINH BA VU⁰¹, INJOON SON⁰², KYUNG TAE KIM⁰¹, SEUNGKI JO^{01*}

INFLUENCE OF SINTERING TEMPERATURE ON THERMOELECTRIC PROPERTIES OF N-TYPE $Bi_{2-x}Sb_xTe_3$ COMPOUNDS

n-type (Bi,Sb)₂Te₃ emerges as a viable alternative to conventional n-type Bi₂(Te,Se)₃, demonstrating superior power generation capabilities when coupled with p-type (Bi,Sb)₂Te₃ in commercial thermoelectric devices. Despite the importance of controlling the donor-like effect in n-type (Bi,Sb)₂Te₃ for optimization of thermoelectric performance, there have been no relevant studies so far. This study focuses on investigating the effect of sintering temperature on the thermoelectric properties of n-type (Bi,Sb)₂Te₃. Increasing the sintering temperature promotes the recovery effect and leads to a reduction in carrier concentration and thereby optimized power factor (2.66 mW m⁻¹ K⁻² at 298 K). Furthermore, the zT value at room temperature increased by 63%, and the highest zT value achieved is 0.52 at 423 K for the sample sintered at 793 K.

Keywords: Bi_{2-x}Sb_xTe₃; thermoelectric; spark plasma sintering; sintering temperature

1. Introduction

Thermoelectric (TE) materials are functional semiconductors that offer a promising solution to energy and environmental challenges through their ability to convert temperature gradients into electrical energy and vice versa [1-3]. The conversion efficiency of TE materials is characterized by a dimensionless figure of merit, $zT = S^2 \sigma T/\kappa$ [4-6], where S, σ , T, and κ represent the Seebeck coefficient, electrical conductivity, absolute temperature, and thermal conductivity, respectively. The κ comprises electronic thermal conductivity (κ_e), lattice thermal conductivity (κ_{lat}), and bipolar thermal conductivity (κ_{bi}) [7]. To improve the zT value, various TE materials have been developed, including Bi₂Te₃-based materials [4,8], half-Heusler alloys [9], skutterudites [10], chalcogenides [11], and oxide materials [12].

Among these materials, Bi_2Te_3 -based compounds, specifically n-type $Bi_2Te_{3-x}Se_x$ and p-type $Bi_{2-x}Sb_xTe_3$, have achieved commercial success due to their superior conversion efficiency near room temperature [1]. However, the disparities in performance and optimal operating temperature ranges between n- and p-type materials [8,13,14] have limited their broader application possibilities. To address this limitation, recent studies have reexamined $Bi_{2-x}Sb_xTe_3$ compounds for their potential as n-type

thermoelectric materials. The alternative n-type compounds exhibit more favorable electronic transport properties compared to conventional $\operatorname{Bi}_2\operatorname{Te}_{3-x}\operatorname{Se}_x$ compounds [15]. The promotion of the donor-like effect due to the facilitated formation of antisite defects enables more effective control over the carrier concentration, resulting in a higher Seebeck coefficient, along with lower κ by larger mass and radius atomic differences [1].

For the fabrication of high-performance TE materials, mechanical alloying (MA) combined with spark plasma sintering (SPS) has been widely adopted due to its ability to control microstructure and composition precisely. The TE properties of Bi₂Te₃-based materials fabricated by MA and SPS are significantly influenced by the sintering conditions through the donorlike effect, which directly determines the carrier concentration - a key parameter governing TE performance optimization. Despite its importance, systematic studies on the effects of sintering conditions, particularly temperature, on the TE properties of *n*-type Bi_{2-x}Sb_xTe₃ remain limited. In this study, we investigate the effects of sintering temperature on the TE properties of *n*-type Bi_{2-x}Sb_xTe₃ compounds. We selected Bi_{1.9}Sb_{0.1}Te₃ as a model system based on its good performance among *n*-type Bi_{2-x}Sb_xTe₃ compounds prepared by powder metallurgical processes.

^{*} Corresponding author: seungkijo@kims.re.kr



¹ KOREA INSTITUTE OF MATERIALS SCIENCE, NANO MATERIALS RESEARCH DIVISION, 797 CHANGWON-DAERO, SEONGSAN-GU, CHANGWON-SI, GYEONGSANGNAM-DO 51508, REPLIBLIC OF KORFA

² KYUNGPOOK NATION UNIVERSITY, DAEGU, KOREA

2. Experimental

The *n*-type Bi_{1.9}Sb_{0.1}Te₃ powder was synthesized by ballmilling method with high impurity (99.999%) bismuth (Bi), antimony (Sb), and tellurium (Te) shots as primary materials. After being weighted according to the stoichiometric ratio, the mixture of materials was ball-milled by a planetary mill (Pulversette 5, Fritsch, Germany). The ball-milling procedure was divided into two stages: the first was carried out at 360 rpm for 48 cycles, followed by the second at the same speed for 24 cycles. The obtained powder was reduced in an H₂ environment at 573 K for 90 minutes. The cylinder bulk samples were fabricated using spark plasma sintering furnace (SPS-210SX, Vacuum Science Laboratory, Korea) at 693 K, 723 K, 753 K, 773 K, and 793 K under 50 Mpa. The crystalline phase of ball-milled powders crystalline phases were detected using X-ray diffraction (XRD) with a Cu $K_{\alpha 1}$ X-ray source (Malvern Panalytical, UK) and the lattice parameters were calculated by Rietveld refinement (Fullprof Suite). SBA458 Nemesis (Netzsch, Germany) measured the temperature-dependent electrical conductivity and Seebeck coefficient from 298 K to 473 K in an argon environment. The Hall carrier concentration (n_H) and Hall carrier mobility (μ_H) were determined using the Van der Pauw configuration utilized by an HMS3500 (Ecopia, South Korea) at room temperature. The formula $\kappa = D\rho C_p$, where D, ρ , and C_p stand for thermal diffusivity, density, and specific heat, was used to calculate the temperaturedependent thermal conductivity. The Archimedes method was used to quantify density, and the laser flash method (NETZSCH, Germany) was used to measure thermal diffusivity. The modified Dulong-Petit law was used to estimate the specific heat [16].

3. Results and discussion

The XRD patterns of the samples prepared at different sintering temperatures are shown in Fig. 1(a). All diffraction peaks are well indexed to Bi₂Te₃ reference pattern (JCPDS#15-0863) without any evidence of secondary phases or impurities. Additionally, no preferred orientation was observed in the (001) planes. The short sintering time and the small grain size from

planetary milling appear to be the main factors contributing to the isotropic crystal structure [17]. Fig. 1(b) displays the calculated lattice parameters a and c of the hexagonal Bi₂Te₃ structure, where a represents the distance between atoms in the basal plane and c corresponds to the height of the unit cell along the stacking direction, revealing that the crystallite size remains nearly constant as the sintering temperature increases, indicating that the sintering temperature has minimal impact on the crystal structure of Bi_{1.9}Sb_{0.1}Te₃.

The electronic transport properties of the samples sintered at 693 K, 723 K, 753 K, 773 K, and 793 K were measured in the direction perpendicular to the sintering pressure and are presented in Fig. 2. The electrical conductivity (σ) increased with increasing sintering temperature up to 753 K, above which it begins to decrease. This decrease can be attributed to the sharp reduction in Hall carrier concentration (n_H) observed at sintering temperatures above 753 K (TABLE 1). The decrease in n_H with increasing sintering temperature could be attributed to the removal of negatively charged carriers through the recovery effect [18]. Similar to other V_2VI_3 compounds, the intrinsic defects in n-type $Bi_{2-x}Sb_xTe_3$ are influenced by the "donor-like effect", which can be expressed as [18]:

$$2V_{\rm Bi}^{""} + 3V_{\rm Te}^{"} + {\rm Bi}_{\rm Te}^{"} \rightarrow V_{\rm Bi}^{""} + {\rm Bi}_{\rm Bi}^{\times} + 4V_{\rm Te}^{"} + 6e'$$

The number of antisite defects and vacancies is constrained by the chemical composition and mechanical energies. Consequently, thermal energy input beyond a critical threshold during powder fabrication no longer promotes the "donor-like effect" [19]. Instead, this excess thermal energy enables Te atoms to return to their initial positions, reducing the concentration of negatively charged carriers through the "recovery effect" – resulting

TABLE 1 Hall carrier concentration (n_H) and Hall carrier mobility (μ_H) of Bi_{1.9}Sb_{0.1}Te₃ measured at room temperature

Sintering temperatures (K)	693 K	723 K	753 K	773 K	793 K
$n_H \times 10^{19} (\text{cm}^{-3})$	10.99	10.59	7.74	6.65	5.76
$\mu_H (\text{cm}^2 \text{V}^{-1} \text{s}^{-1})$	103.85	117.53	151.42	162.99	186.62

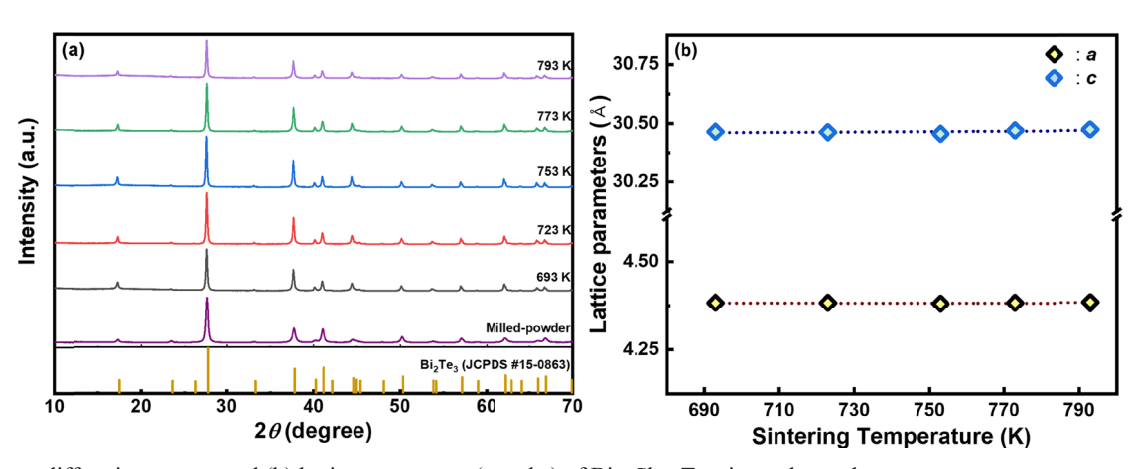


Fig. 1. (a) X-ray diffraction pattern and (b) lattice parameters (a and c) of $Bi_{1.9}Sb_{0.1}Te_3$ sintered sample

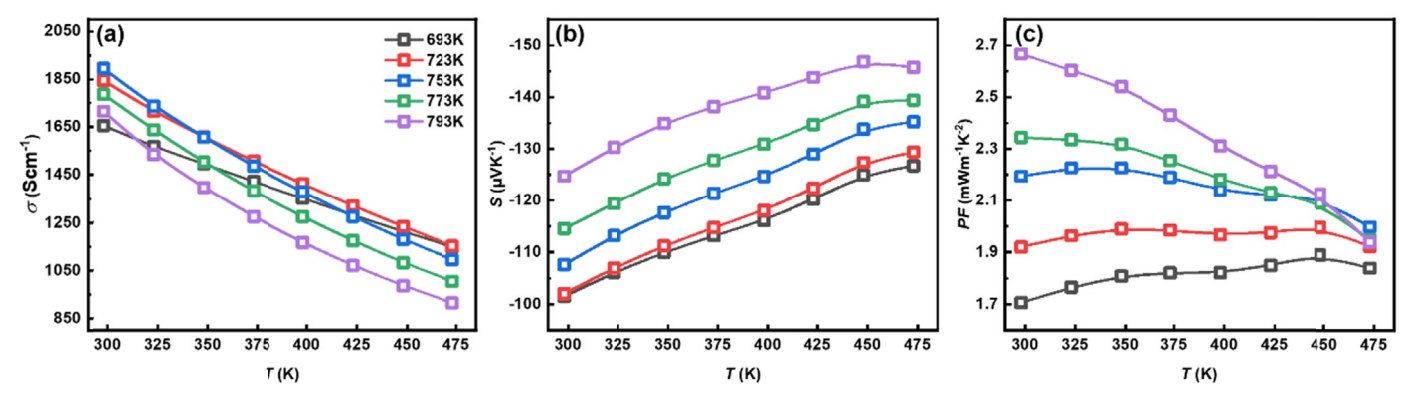


Fig. 2. Temperature dependence of (a) Electrical conductivity (b) Seebeck coefficient (c) Power factor of spark plasma sintered Bi_{1.9}Sb_{0.1}Te₃

in a significant decrease in carrier concentration. On the other hand, the enhancement of the recovery effect is also considered a significant contributing factor to the observed increase in carrier mobility in this study. This is primarily due to the reduction in crystalline disorder [20], along with accompanying changes in microstructure, density, and grain size induced by higher sintering temperatures.

The Seebeck coefficient (S) is highly dependent on the carrier concentration, and exhibits significant sensitivity to sintering temperature (Fig. 2(b)). The negative S values indicate that all samples are n-type characteristics. The absolute value of S shows a modest increase as the sintering temperature rises from 693 K to 723 K, followed by a substantial increase with each subsequent temperature increment. This trend shows a strong correlation with the observed decrease in n_H , indicating a pronounced recovery effect. Fig. 2(c) shows the temperature-dependent power factor (PF). The sample sintered at 793 K exhibits a maximum PF value of 2.66 mW m⁻¹ K⁻² at 298 K, representing a 41% enhancement compared to the sample sintered at 693 K. This significant enhancement in PF can be attributed to the optimized carrier concentration, which establishes an effective balance between σ and S.

The electronic band parameters obtained through the single parabolic band (SPB) model are presented in Fig. 3. The values of the density of state effective mass (m_d^*) and nondegenerate mobility (μ_0) were calculated by comparing the theoretical SPB curves with the measured S, S, S, and S, and S, and S, are defined as follows [21]:

$$S = \frac{k_B}{e} \left(\eta - \frac{2F_1(\eta)}{F_0(\eta)} \right) \tag{1}$$

$$n_{H} = \frac{16\pi}{3} \left(\frac{2m_{d}^{*}k_{B}T}{h^{2}} \right)^{3/2} \frac{\left(F_{0}(\eta)\right)^{2}}{F_{-1/2}(\eta)}$$
 (2)

$$\mu_{H} = \mu_{0} \frac{F_{-1/2}(\eta)}{2F_{0}(\eta)} \tag{3}$$

$$F_{j}(\eta) = \int_{0}^{\infty} \frac{\varepsilon^{j} d\varepsilon}{1 + \exp[\varepsilon - \eta]}$$
 (4)

where k_B , e, F_j , and η present Boltzmann constant, elemental electric charge, Fermi integral of order j, and reduced Fermi energy, respectively. The calculations of m_d^* reveal no notable variation with sintering temperature, maintaining a consistent value of $\sim 1.1~m_0$. For μ_0 , the calculated results indicate that the sample sintered at 793 K exhibits the highest value. μ_0 reaches 292 cm² V⁻¹ s⁻¹ and gradually decreases to 180 cm² V⁻¹ s⁻¹ for the sample sintered at 693 K. The prediction of $n_{\rm H}$ dependent PF and the weighted mobility, were performed using the theoretically determined μ_0 and m_d^* and presented in Fig. 3(c,d). The weighted mobility is calculated using the following formula [22]:

$$\mu_w = \mu_0 \times m_d^{*3/2} \tag{6}$$

the μ_w increases with the sintering temperature, reaching a maximum value of 343 cm 2 V $^{-1}$ s $^{-1}$ for the sample sintered at 793 K. Since μ_w is proportional to the theoretical maximum PF [29], the predicted maximum value of PF exhibits a corresponding increase with sintering temperature. This maximum value can be achieved through carrier concentration optimization. Based on the SPB model predictions, the maximum attainable PF at room temperature is 2.85 mW m $^{-1}$ K $^{-2}$ at a $n_{\rm H}$ of 2.69 × 10 19 cm $^{-3}$. Although the experimentally measured PF is 2.66 mWm $^{-1}$ K $^{-2}$, there remains potential for a 7% enhancement.

The temperature-dependent total thermal conductivity (κ) is presented in Fig. 4(a). The κ shows a trend similar to that of the electrical conductivity, indicating a significant contribution from the electronic thermal conductivity (κ_e). The κ_e was calculated based on the Wiedemann-Franz law ($\kappa_e = L_0 \sigma T$), where L_0 is Lorenz number (in 10^{-8} W Ω K⁻²) and determined by the equation proposed by Kim et al [23]. Fig. 4(b) shows temperature dependent $\kappa - \kappa_e$. While the $\kappa - \kappa_e$ values show minimal variation at room temperature, samples sintered at higher temperatures exhibit elevated $\kappa - \kappa_e$ values at higher temperatures. This suggests an enhanced bipolar contribution to κ due to the reduction in n_H .

The temperature-dependent figure of merit (zT) values are presented in Fig. 4(c). The zT values increase with sintering temperature, achieving a maximum value of 0.52 at 423 K for the sample sintered at 793 K, representing a 12% enhancement compared to the sample sintered at 693 K. Notably, peak zT shifts toward room temperature with increasing sintering temperature. The n_H -dependent zT curves indicate that higher sin-

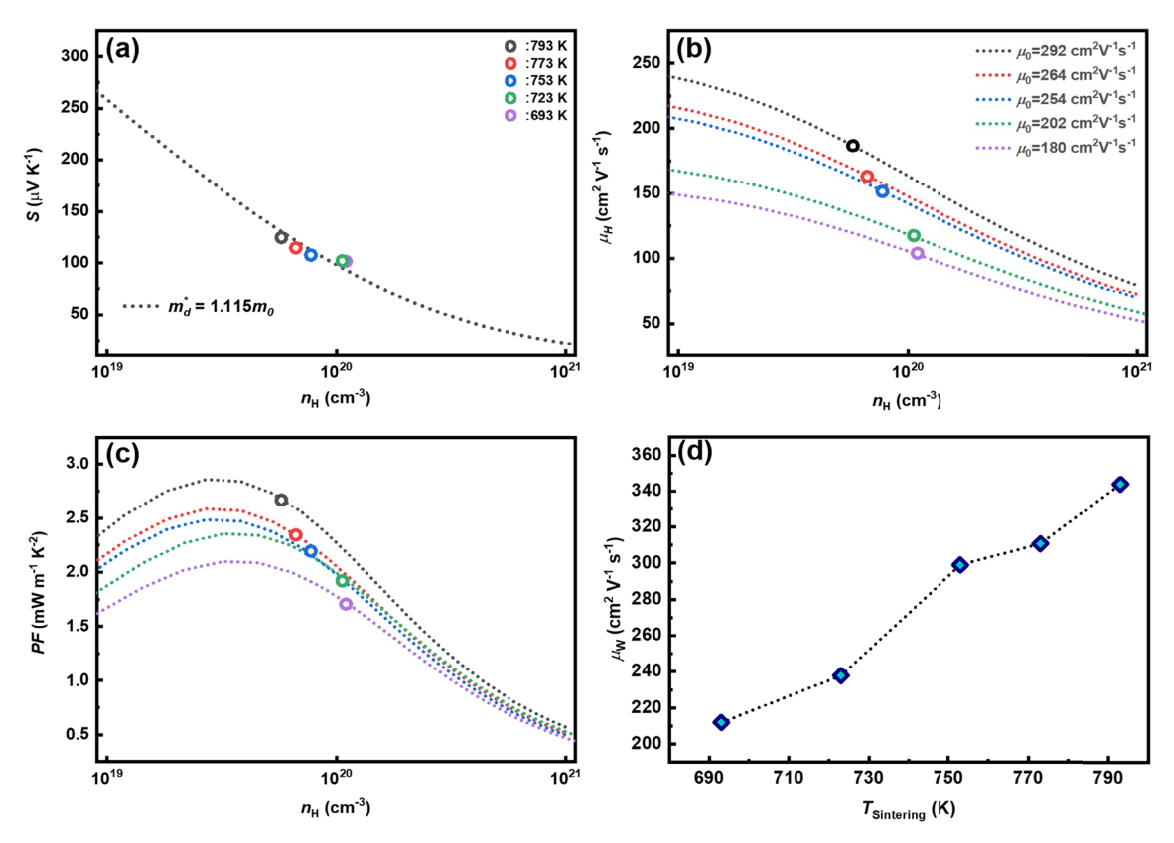


Fig. 3. Carrier concentration dependence of (a) Hall carrier mobility (b) Seebeck coefficient (c) Power factor, and (d) sintering temperature dependence of weighted mobility of $Bi_{1.9}Sb_{0.1}Te_3$

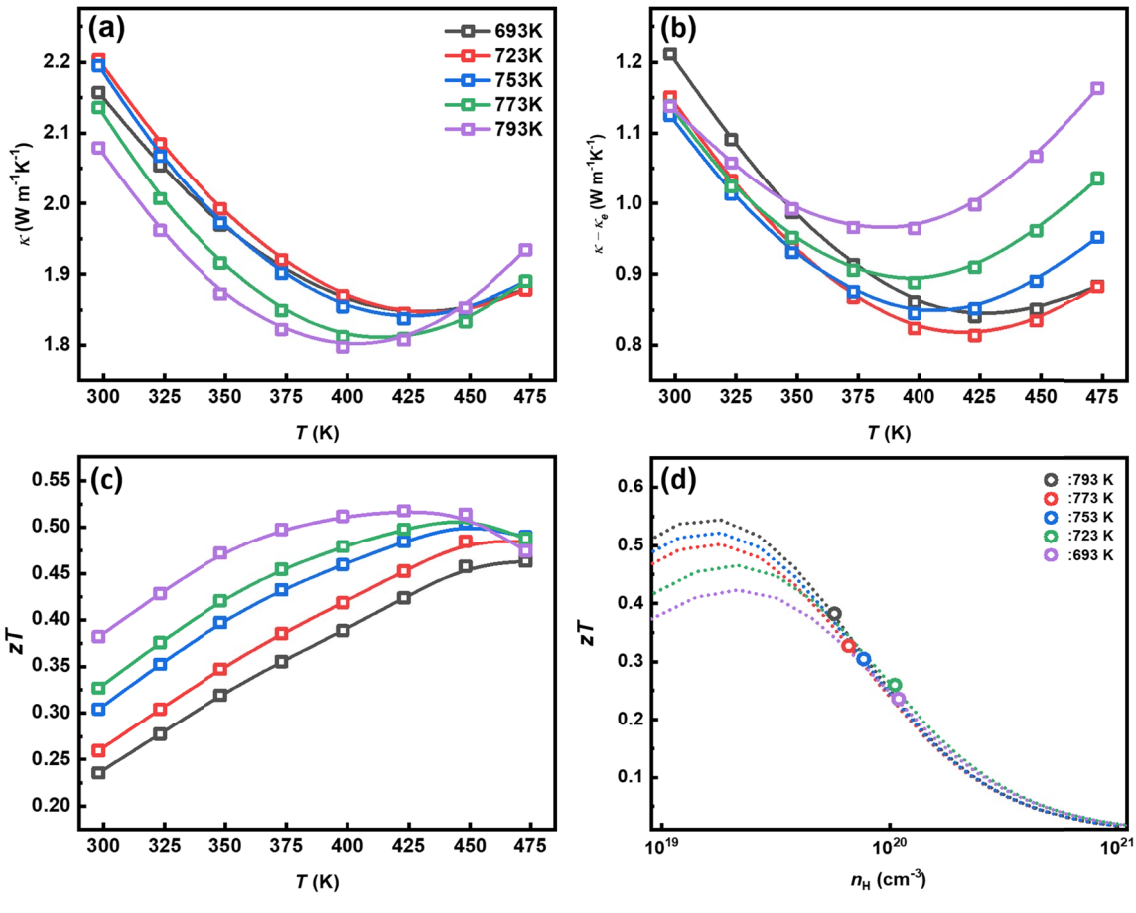


Fig. 4. Temperature dependence of (a) total thermal conductivity (b) $\kappa - \kappa_e$ (c) Figure of merit zT, and (d) carrier concentration dependence of zT of $\mathrm{Bi}_{1.9}\mathrm{Sb}_{0.1}\mathrm{Te}_3$

tering temperatures facilitate the optimization of n_H , leading to enhanced zT values. According to the SPB model predictions, the maximum theoretical zT attainable at room temperature could be 42% higher than the experimentally achieved value in this study (Fig. 4(d)).

4. Conclusion

In this study, the influence of sintering temperature on the thermoelectric properties of $Bi_{1.9}Sb_{0.1}Te_3$ was investigated. Experimental results indicate that as the sintering temperature increases, the recovery effect is promoted, leading to a decrease in carrier concentration and an increase in carrier mobility. Consequently, the Seebeck coefficient and power factor improved at room temperature. Additionally, the thermal conductivity showed minimal variation and tends to follow a trend similar to that of electrical conductivity. The results reveal that the sample sintered at the highest temperature of 793 K exhibits the best electronic transport properties with a weighted mobility μ_w of 343 cm² V⁻¹ s⁻¹ and the highest thermoelectric performance with a zT of 0.52 at 423 K, which is 12% higher compared to the sample sintered at 693 K.

REFERENCES

- [1] L.B. Vu, Exploring Thermoelectric Transport Properties and Band Parameters of n-Type Bi_{2-x}Sb_xTe₃ Compounds Using the Single Parabolic Band Model. J. Powder Mater. 31, 119-125 (2024). DOI: https://doi.org/10.4150/jpm.2024.00045
- [2] J.M. Park, Investigation of the Thermal-to-Electrical Properties of Transition Metal-Sb Alloys Synthesized for Thermoelectric Applications. J. Powder Mater. 31, 236-242 (2024). DOI: https://doi.org/10.4150/jpm.2024.00031
- [3] H.S Lee, Recent progress on Performance Improvements of Thermoelectric Materials using Atomic Layer Deposition. J. Powder Mater. 29 (1), 56-62 (2022).
 DOI: https://doi.org/10.4150/kpmI.20
- I.T. Witting, The Thermoelectric Properties of Bismuth Telluride.
 Adv. Electron. Mater. 5, 1800904 (2019).
 DOI: https://doi.org/10.1002/aelm.201800904
- [5] S.H. Jung, Enhancement of Thermoelectric Performance in Spark Plasma Sintered p-Type Bi_{0.5}Sb_{1.5}Te₃ Compound via Hot Isostatic Pressing (HIP) Induced Reduction of Lattice Thermal Conductivity. J. Powder Mater. 30, 123-129 (2023). DOI: https://doi.org/10.4150/kpmi
- [6] M.J. Joeng, Thermoelectric Performance Enhancement of Sintered Bi-Te Pellets by Rotary-type Atomic Layer Deposition. J. Powder Mater. 30 (2), 130-139 (2023). DOI: https://doi.org/10.4150/kpmi.2023.30.2.130
- H.S. Kim, Understanding bipolar thermal conductivity in terms of concentration ratio of minority to majority carriers. J. Mater. Res. Technol. 14, 639-646 (2021).
 DOI: https://doi.org/10.1016/j.jmrt.2021.06.087

- [8] S.I. Kim, Dense dislocation arrays embedded in grain boundaries for high-performance bulk thermoelectrics. Science 348, 109-114 (2015). DOI: https://doi.org/10.1126/science.aaa4166
- [9] K. Xia, Half-Heusler thermoelectric materials. Appl. Phys. Lett. 118, 140503 (2021).
 - DOI: https://doi.org/10.1063/5.0043552
- [10] Y. Mona, Development of Skutterudite-Type Thermoelectric Materials La_xCo₄Sb₁₂ Using High-Pressure Synthesis Method. JOM. 76, 153-159 (2024).
 - DOI: https://doi.org/10.1007/s11837-023-06150-5
- [11] S.Y. Tee, Thermoelectric Silver-Based Chalcogenides. Adv. Sci. 9, 2204624 (2022).
 - DOI: https://doi.org/10.1002/advs.202204624
- [12] M. Zhu, Enhancement of thermoelectric properties in $Sr_{0.7}Ba_{0.3}$ Nb₂O_{6- δ}-based ceramics via nano-sized Ti as additive. J. Appl. Phys. **135**, 025103 (2024).
 - DOI: https://doi.org/10.1063/5.0177326
- [13] G. Yang, Enhanced thermoelectric performance and mechanical strength of n-type BiTeSe materials produced via a composite strategy. Chem. Eng. J. 428, 131205 (2022). DOI: https://doi.org/10.1016/j.cej.2021.131205
- [14] Z.L. Wang, Improved Thermoelectric Properties of Hot-Extruded Bi-Te-Se Bulk Materials with Cu Doping and Property Predictions via Machine Learning. Adv. Electron. Mater. 5, 1900079 (2019). DOI: https://doi.org/10.1002/aelm.201900079
- [15] Y. Zhou, n-Bi_{2-x}Sb_xTe₃: A Promising Alternative to Mainstream Thermoelectric Material n-Bi₂Te_{3-x}Se_x near Room Temperature. ACS Appl. Mater. Interfaces. **12**, 31619-31627 (2020). DOI: https://doi.org/10.1021/acsami.0c07566
- [16] K.A. Borup, Measuring thermoelectric transport properties of materials. Energy Environ. Sci. 8, 423-435 (2015). DOI: https://doi.org/10.1039/c4ee01320d
- [17] Y. Sun, Strategies to Improve the Thermoelectric Figure of Merit in Thermoelectric Functional Materials. Front Chem. 10, 865281 (2022). DOI: https://doi.org/10.3389/fchem.2022.865281
- [18] T. Zhu, New Insights into Intrinsic Point Defects in V2VI3 Thermoelectric Materials. Adv. Sci. 3, 1600004 (2016).DOI: https://doi.org/10.1002/advs.201600004
- [19] L.P. Hu, Improving thermoelectric properties of n-type bismuth—telluride-based alloys by deformation-induced lattice defects and texture enhancement. Mater. Res. Bull. **99**, 377-384 (2018). DOI: https://doi.org/10.1016/j.actamat.2012.05.008
- [20] L. Hu, Point Defect Engineering of High-Performance Bismuth-Telluride-Based Thermoelectric Materials. Adv. Funct. Mater. 24, 5211-5218 (2014).
 - DOI: https://doi.org/10.1002/adfm.201400474
- [21] H. Park, Theoretical Maximum Thermoelectric Performance of p-Type Hf- and Zr-Doped NbFeSb Half-Heusler Compounds. Adv. Electron. Mater. 10, 2300857 (2024). DOI: https://doi.org/10.1002/aelm.202300857
- [22] G.J. Snyder, Weighted Mobility. Adv. Mater. 32, e2001537 (2020). DOI: https://doi.org/10.1002/adma.202001537
- [23] H.S. Kim, Characterization of Lorenz number with Seebeck coefficient measurement. APL Mater. 3, 041506 (2015).
 DOI: https://doi.org/10.1063/1.4908244